*Article*

# Nucleation and Growth of Tin-Zinc Electrodeposits on a Polycrystalline Platinum Electrode in Tartaric Acid

*Allan da S. Taguchi, Fábio R. Bento and Lucia H. Mascaro\**

*Departamento de Química, Universidade Federal de São Carlos, CP 676, 13565-905, São Carlos-SP, Brazil*

Medidas de transientes de corrente e microscopia eletrônica de varredura foram utilizados para caracterizar o processo de eletrocristalização e morfologia de ligas de estanho-zinco eletrodepositadas sobre Pt, na ausência e na presença de ácido tartárico. O modelo de Scharifker e Hills foi utilizado para analisar os transientes de corrente e revelou que o processo de eletrocristalização da liga Sn-Zn na presença de tartarato, sob as condições estudadas, é governado por nucleação progressiva tridimensional controlada por difusão. Na ausência do complexante, os resultados indicaram que o processo de nucleação varia de instantâneo para progressivo à medida que o potencial de deposição torna-se mais negativo, ou seja, pela incorporação de zinco ao depósito. Os resultados de microscopia mostraram depósitos com duas camadas com morfologias diferentes e que a mesma sofre influência do potencial de deposição

Current transients measurements and scanning electron microscopy were used to characterize the electrocrystallization process and morphology of tin-zinc alloys electrodeposited on Pt, in the absence and in the presence of tartaric acid. The model of Scharifker and Hills was used to analyze the current transients and it revealed that Sn-Zn electrocrystallization process in the presence of tartrate, under the studied conditions, is governed by three-dimensional progressive nucleation controlled by diffusion. In the absence of the complexant, the results indicated that nucleation process changes from instantaneous to progressive when the deposition potential becomes more negative, or when the incorporation of zinc occured to the deposit. The microscopic results showed deposits with two layers with different morphologies and is also influenced by deposition potential.

**Keywords:** tin, zinc, alloy, electrodeposition, electrocrystallization

## Introduction

Tin is non-toxic, has excellent resistance to corrosion and provides an even, solderable coating on most metals. Although hot tin dipping is the simplest application method, dipping components in a molten tin bath provide little control over thickness. Electroplating tin from an aqueous solution improve greater thickness control even on complex shapes, witch ability to control visual appearance. Tin can also be electroplated and has a wide utilities in both decorative and functional applications. During electrodeposition, tin readily forms alloys with other metals such as zinc, lead, bismuth, copper, and silver.[1-10] The availability of new improved tin alloys with zinc has provided coatings with unique properties with particular value in the automotive industry. Tin-zinc alloy coatings have good corrosion resistance, frictional properties and ductility, and good solderability.[11,12] In view of their good

properties, they proposed as substitutes for other industrial coatings, such as those of cadmium (toxic) and nickel (allergenic).[11,12] Tin-zinc coatings have been used on chassis of electrical and electronic apparatus and on critical automotive parts, such as fuel and brake line components. Thus, studies the formation of metallic films have great importance, since one must control the growth process according to the desired application.

Tin-zinc electrodeposition has been investigated using different bath systems, different complexing agents (tartrate, gluconate, peptones etc), additives and pH values, in order to replace contaminant cyanide baths used in industrial processes for Sn-Zn alloy plating.[12-16] These papers reported the conditions to obtain alloys with the eutectic composition Sn-9Zn or alloys coatings with 20-30% Zn, which have the best mechanical and corrosion properties. Guaus and Torrent-Burgués investigated tin-zinc alloy electrodeposits obtained from sulphate-gluconate and sulphate-tartrate baths.[11,12] These authors concluded that the zinc content in the alloy increases by using tartrate

*\*e-mail: lmascaro@power.ufscar.br*

as complexing agent instead of gluconate. Ashiru and Shirokoff used an alkaline bath (pH 12-13 and temperature of 40-80ºC) and tartrate as complexant to obtain 70/30 to 80/20 tin/zinc alloy compositions.[3] These authors observed that the microstructure consisted of small particles of zinc in a tin matrix and concluded that the (80/20) tin-zinc electroplated coating provided superior protection to corrosion when compared to zinc, (90/10) zinc/nickel and cadmium coatings. Vitkova *et al.*[2] aimed at the deposition of high quality Zn-Sn coatings with the minimum possible tin content (up to 20%). The Zn-Sn coatings were deposited from gluconate and citrate medium. They also concluded that the best protection properties are obtained with alloys containing more than 20% tin. Vasantha *et al.*[13] used baths with Sn:Zn molar ratios of 80:20, 60:40, 40:60 and 20:80 in medium containing sodium gluconate and peptone. These authors observed that increasing the gluconate concentration, pH and temperature of the 60:40 baths there was an increase in the tin content of the alloy. Some authors, using sequential experiments strategies, proposed robust depositing settings for the electroplating of Sn-Zn deposits with the composition close to the eutectic point.[17,18] Electrodeposition of Sn-Zn alloys from ionic liquids has also been reported.[14,19,20]

In spite of the few existent papers about the Sn-Zn alloy electrodeposition process, most of them report the dependence of the alloy composition on the variables of the process. It was not found in the literature papers about kinetics of the alloy deposition, mainly those concerning electrocrystallization process. However, one way to evaluate the formation of metallic films through the electrodeposition process involves electrochemical studies of the nucleation and growth processes. One theoretical model was developed by Scharifker and Hills.[21] According to them, the formation of bi or three-dimensional nuclei is controlled by diffusion and the nucleation process may be considered instantaneous or progressive. This model has been applied with success for several electrodeposition systems, as: Ni, Cu, Co-Fe, Zn-Fe, Ni-Fe, Cu-Pb among others.[22-27]

The aim of this study was to characterize the first stages of tin-zinc deposits in absence and presence of tartaric acid used as complexing agent. The electrochemical behavior of alloys coatings was analyzed using cyclic voltammetry and current transients. Surface morphology and composition were evaluated by scanning electron microscopy (SEM) and electron dispersive analysis (EDX), respectively.

## Experimental

Electrochemical experiments were carried out with a three-electrode system using a microcomputer-controlled EG&G PARC potenciostat/galvanostat model 283. The working electrode was a 0.071 cm$^2$-area platinum disk sealed into a glass tube, the counter electrode was a platinum spiral and the reference one was an 3.0 mol L$^{-1}$ Ag|AgCl|KCl electrode. The platinum electrodes were polished up to a mirror finishing using 1 μm alumina powder and cleaned with deionized water. The electrodes were then cleaned in a sulphonitric solution and rinsed thoroughly with deionized water.

Chemicals used, like SnSO$_4$, ZnSO$_4$.7H$_2$0, tartaric acid (C$_4$H$_6$O$_6$) and Na$_2$SO$_4$, were of analytical grade. All solutions were freshly prepared with low conductance water purified in a Millipore Milli-Q system. The electrolytic compositions are listed in Table 1. All baths contained 1.0 mol L$^{-1}$ Na$_2$SO$_4$ as the supporting electrolyte and had their pH adjusted to 4.5 using NaOH, except those containing SnSO$_4$ in the absence of tartaric acid. All experiments were performed at room temperature.

**Table 1.** Electrolytic composition for Sn-Zn electrodeposition bath

| Bath | [SnSO$_4$]/ (mol L$^{-1}$) | [ZnSO$_4$.7H$_2$0]/ (mol L$^{-1}$) | [Na$_2$SO$_4$]/ (mol L$^{-1}$) | [tartaric acid]/ (mol L$^{-1}$) |
|---|---|---|---|---|
| I | 0.02 | 0.02 | 1.0 | - |
| II | 0.02 | 0.02 | 1.0 | 0.12 |

Several voltammetric experiments were carried out at 50.0 mV s$^{-1}$ with 0.00 V as initial potential value scanning towards negative potentials in order to determine the potential windows which each metal was deposited. The nucleation process was evaluated by potentiostatic steps within the potential windows where the deposition processes were observed. The potentiostatic steps were carried out from 0.00 V (initial potential) to different final potential ($E_f$) values, which were previously chosen from voltammetric curves. The length of the potentiostatic steps was 1.0 s, and then, for zinc and tin-zinc alloy in the absence of tartaric acid 3.0 s for a better observation of their behaviors. The chronoamperometric experiments were carried out twice and showed the same results.

The composition and morphology of deposits were examined using an EDX analyzer integrated with ZEISS model DSM 960 scanning electron microscope (SEM). Tin, zinc and tin-zinc deposits were grown potentiostatically at different deposition potentials during 20 min. The same deposits were also grown until reach the charge density ($q$) of 1.0 C cm$^{-2}$ and 3.0 C cm$^{-2}$.

# Results and Discussion

*Voltammetric results*

Initially, cyclic voltammetry experiments were used to evaluate the deposition and dissolution processes of Sn-Zn alloys in the presence and absence of tartaric acid. These studies were performed in 0.02 mol L$^{-1}$ SnSO$_4$, 0.02 mol L$^{-1}$ ZnSO$_4$, 1.0 mol L$^{-1}$ Na$_2$SO$_4$ and in presence and absence of 0.12 mol L$^{-1}$ C$_4$H$_6$O$_6$ solutions. Cyclic voltammograms (CVs) obtained are shown in Figure 1, together with the CVs of the individual metals for comparison.

In Figure 1 it is possible to conclude that the presence of tartaric acid affect electrodeposition process. In the absence of tartaric acid two cathodic peaks were observed followed by current increase at more negative potential due to hydrogen evolution reaction. Comparing the CVs for Sn-Zn alloy (solid lines) with those for individual ions at the same concentration, a first cathodic peak, at -0.67 V, corresponds to Sn (II) reduction and the ones around -1.20 V to Zn (II) reduction. In the presence of tartaric acid the cathodic peak attributed to Sn (II) reduction shifts to more positive potential indicating that when tartrate anion is added in the solution, Sn deposition is favored. This behavior is due to the complex formed with this metal ion and tartrate anion as pointed by Gauss and Torrent-Burgues.[11,12] By the other hand, the peak corresponding to Zn (II) reduction is shifted to more negative potential and it is not defined.

Analyzing the anodic scans, it is possible to observe several stripping peaks. In the tartaric acid absence, one shoulder and one main peak is observed. For pure Sn, the anodic scan presents one dissolution peak at -0.36 V, therefore in the potential region where appears the shoulder in the CVs for Sn-Zn. For pure Zn a broad peak

is observed at -0.70 V, but the dissolution charge is very low, indicating that little Zn was deposited. In the presence of the complexing agent the voltammetric profile presents more complex form with several anodic peaks between -0.70 and 0.00 V, these peaks can be associated to different phases and/or alloy compositions.[28] Major discussions about anodic peaks need further studies.

We could also observe in Figure 1 that the dissolution charge in the tartrate presence is much larger than in its absence, therefore, in the presence of tartaric acid the reduction process is favored. The voltammograms show crossovers between the currents of the positive and negative sweeps, which suggest the presence of a nucleation and growth process.[26]

*Morphology and composition analysis*

Coatings of Sn-Zn on Pt substrate obtained at different potentials deposition, maintaining the charge density constant (1.0 C cm$^{-2}$) to have films of same thickness, were analyzed by SEM and EDX. The deposit conditions were chosen from the previous voltammetric experiments to obtain deposits with different characteristics. Figure 2 presents the SEM micrographs of (A) and (B) pure tin deposited at -0.70 V and (C) and (D) pure zinc deposited at -1.50 V. Figures 3 (A)-(H) presents the SEM micrographs of the tin-zinc films deposited at -0.70, -0.95, -1.20 and -1.50 V from solutions specified in Table 1, in the absence [(A), (C) , (E) and (G)] and in the presence of tartaric acid [(B), (D), (F) and (H)].

In Figure 2 it can be seen that the morphology of Zn deposits is quite different from that of Sn deposits. Sn coating is more compact with polyhedral crystallites shape and Zn coating is of the type needles and less compact. The morphology of Sn film does not change significantly in the tartrate presence, however it was not possible to observe the
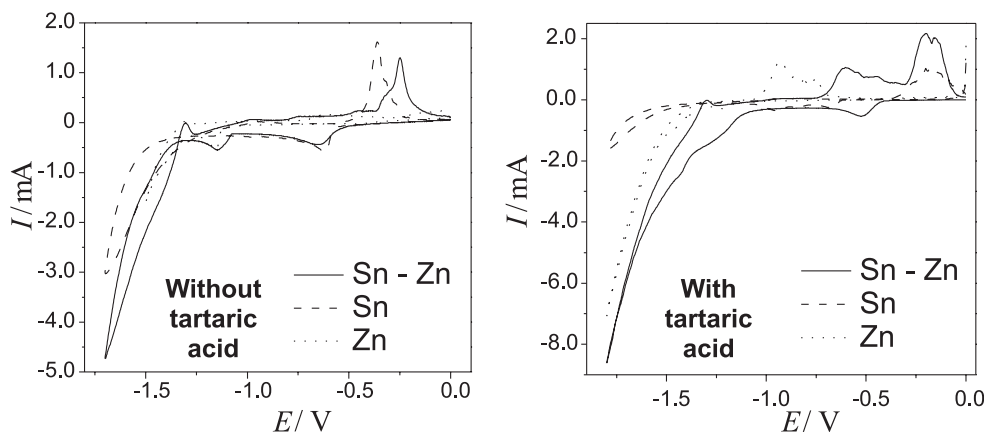


**Figure 1.** Cyclic voltammograms at 50 mV s$^{-1}$ for solutions containing 1.0 mol L$^{-1}$ Na$_2$SO$_4$ + 0.02 mol L$^{-1}$ SnSO$_4$ and/or 0.02 mol L$^{-1}$ ZnSO$_4$·7H$_2$O in the absence and presence of 0.12 mol L$^{-1}$ C$_4$H$_6$O$_6$ (tartaric acid) on Pt electrode.
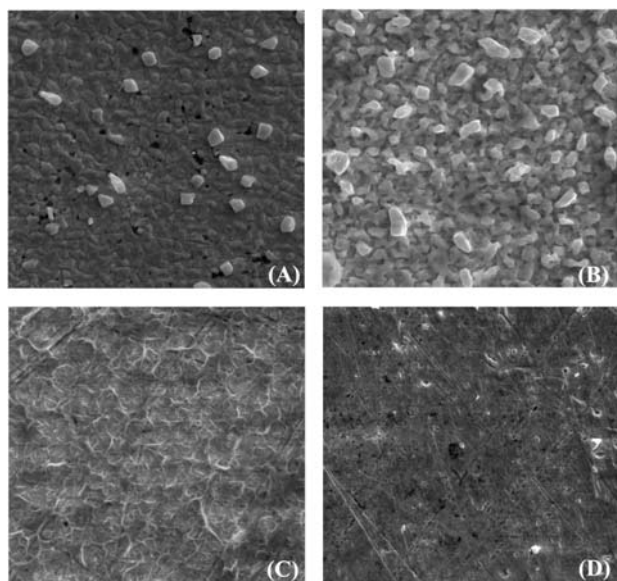
**Figure 2.** SEM images deposits obtained potentiostatically for Sn at **-**0.60 V (A) and (B) and for Zn at -1.50 V (C) and (D) from bath compositions specified in Table 1.

zinc deposit in the presence of tartaric acid [Figure 2 (D)], probably of absence of enough deposition potential under this condition. Figure 3 is shows that the deposit morphology changes significantly with the deposition potential (except to -0.70 and -0.95 V) but it is little affected by the presence of tartaric acid. In -0.70 and -0.95 V, the deposits form a uniform coating with a fine microstructure under both conditions, absence [Figures 3 (A) and (C)] and presence [Figures 3 (B) and (D)] of tartaric acid. However, in Figures 3 (A) and (C) (without tartrate) an inferior and a superior deposit can be observed in this micrography. Lower inferior deposit shows coalescence of crystallites and upper have polyhedral crystallites shape. The same morphology is observed for pure Sn deposits. At more negative deposition potential the deposits also present two layers in wich the number of superior crystals is higher and has different crystallite morphology and the lower coating is more compact. At -1.50 V the growth of second layer seems to be inhibited in the absence of tartaric acid. This fact is in accordance to the voltammetric results (Figure 1) because at this potential it is already possible to observe that the contribution of the hydrogen evolution reaction is so significant that inhibits the alloy deposition. On the other hand, in tartrate presence and deposition potential of -1.50 V, the amount of crystals is higher, again in agreement with cyclic voltammetry results observed in Figure 1 (with tartaric acid).

Table 2 shows the atomic compositions of the tin-zinc alloys deposited at the same conditions of those in Figure 3, obtained from EDX analysis. No Zn was deposited at -0.70 and -0.95 V, consistent with the voltammogramms results seen in Figure 1, where Sn is deposited around
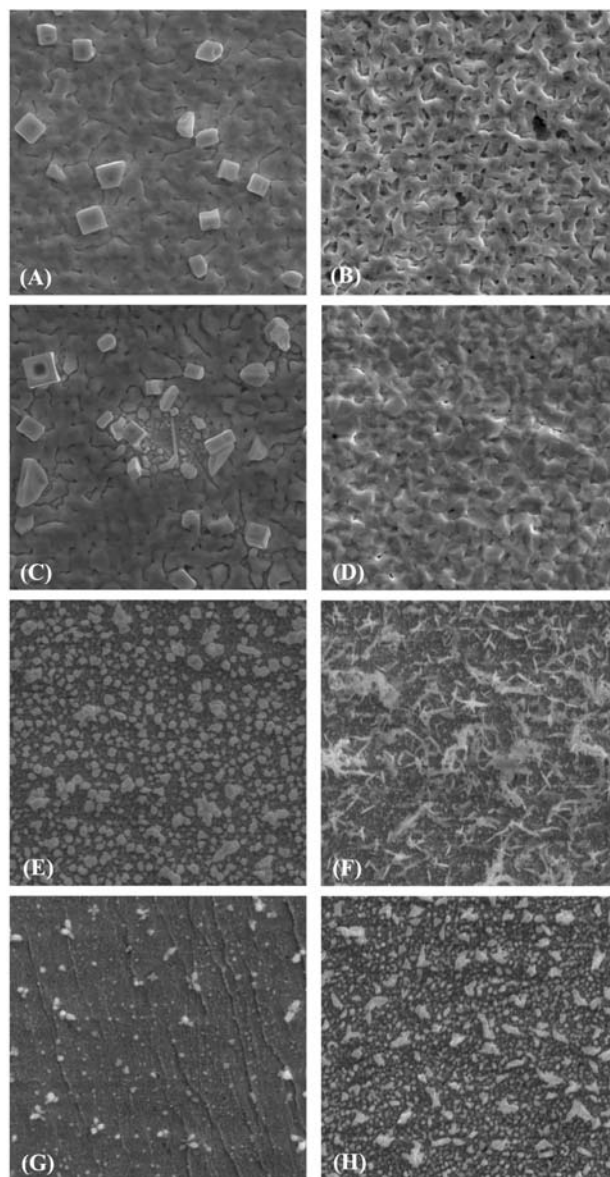


**Figure 3.** SEM images of Sn-Zn deposits obtained potentiostically at (A) and (B) -0.70 V, (C) and (D) -0.95 V, (E) and (F) -1.20 V and (G) and (H) -1.50 V from bath compositions specified in Table 1.

-0.70 V and Zn around -1.20 V. At more negative potentials, -1.20 and -1.50 V, both Zn and Sn are deposited. Actually, Zn can be detected in the film starting from a deposition potential of -1.00 V. As it can be observed in Table 2, for more negative deposition potentials, Sn contents decreases when deposition potential is more negative in the presence of tartaric acid. An opposite behavior is observed in the tartrate absence. These results may indicate that the tartrate presence in the deposition bath, besides favoring the alloy deposition, as previously discussed, also increases the content of Zn in the deposits. These results are in accordance with that observed by Guaus and Torrent-Burgués.[11]

**Table 2.** Atomic compositions of the Sn-Zn coatings deposited potentiostically at different potentials under charge control (1.0 C cm$^{-2}$) from bath composition specified in Figure 1

| Bath | $E_{dep}$ / V | Sn% (at/at) | Zn% (at/at) |
|---|---|---|---|
| Solution I | -0.70 | 100 | – |
| | -0.95 | 100 | – |
| | -1.20 | 55 | 45 |
| | -1.50 | 70 | 30 |
| Solution II | -0.70 | 100 | – |
| | -0.95 | 100 | – |
| | -1.20 | 66 | 34 |
| | -1.50 | 60 | 40 |

*Transients analysis*

Although some of the cyclic voltammograms in Figure 1 do not exhibit the current crossover, which is indicative of an overpotential driven nucleation process, chronoamperometric experiments revealed that the deposition of Sn-Zn on Pt electrode involves nucleation/growth processes. In these experiments, the Pt electrode potential stepped from an initial value where no reduction of Sn or Zn would take place to potentials sufficiently negative to initiate nucleation/growth process. A collection of the current–time transients for the electrodeposition of Sn-Zn (between -0.70 and -1.20 V) in the absence and presence of tartaric acid is shown in Figures 4 (A) and (B).

In Figures 4 (A) and (B), the current transients showed the expected behavior (current increases rapidly to a maximum, $I_{max}$ and $t_{max}$, due to the nucleation and growth of nuclei and then decreases gradually with time, corresponding to linear diffusion). These curves present a typical response of a three-dimensional (3D) multiple nucleation with diffusion controlled growth.[21] Kinetics information about electrocrystallization process could then be obtained by analyzing the rising portion and the maximum of the experimental current transients. Comparing Figures 4 (A) and (B), for the same final potential, $I_{max}$ is larger and $t_{max}$ is lower, in the tartrate presence. This fact seems to indicate that the complexant accelerate the nucleation process. This effect can be explained by the ligands species formed with Sn(II), that favor the deposition process.[11]

These transients were normalized to $(I/I_{max})^2$ *vs.* $t/t_{max}$ and then compared to the well known theoretical $(I/I_{max})^2$ *vs.* $t/t_{max}$ curves derived for instantaneous and progressive three-dimensional (3D) nucleation/growth models,[21] whose equations are given for instantaneous nucleation:

$$\left(\frac{I}{I_{max}}\right)^2 = \frac{1.9542}{t/t_{max}}\left\{1-\exp\left[-1.2564\left(\frac{t}{t_{max}}\right)\right]\right\}^2 \tag{1}$$

and for progressive nucleation

$$\left(\frac{I}{I_{max}}\right)^2 = \frac{1.2254}{t/t_{max}}\left\{1-\exp\left[-2.3367\left(\frac{t}{t_{max}}\right)^2\right]\right\}^2 \tag{2}$$

Non-dimensional plots obtained with the experimental and theoretical data for tin-zinc alloy deposition in the absence and in the presence of tartaric acid are shown in Figures 5 (A) and (B), respectively.

It is clear from Figure 5 (B) that Sn-Zn alloy deposition on Pt follows the theoretical response for a progressive nucleation, over all the measured potential. However, in the tartrate absence [see Figure 5 (A)] the normalized experimental curves are located between instantaneous and progressive nucleation theoretical curves. In more positive potentials (-0.7 V), where pure Sn is deposited (see Table 2), the electrocrystallization process happens through instantaneous nucleation. As soon as the final potential turns to more negative values, the nucleation process changes from instantaneous to progressive. From these results we could say that as soon as Zn is being incorporated to the deposits, the nucleation process is modified.
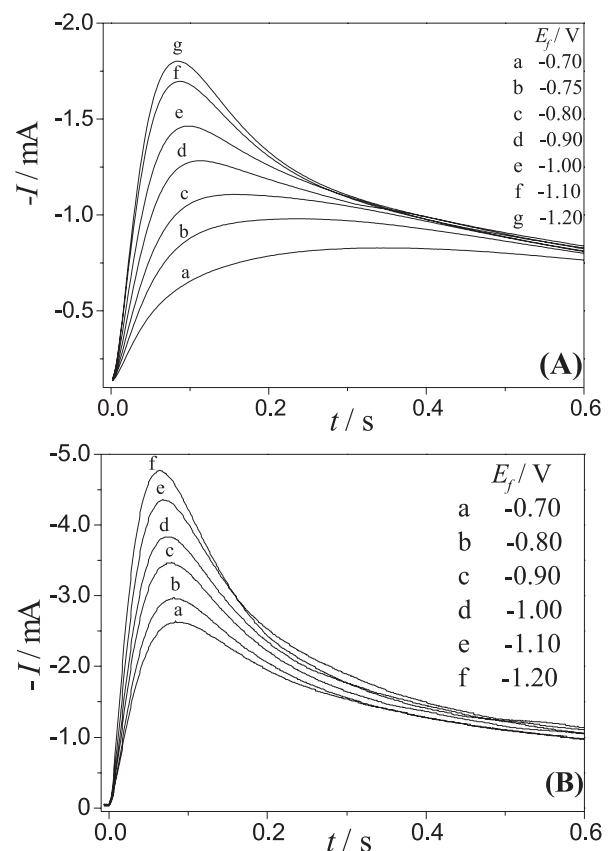


**Figure 4.** Current transients for Sn-Zn deposition from 0.02 SnSO$_4$ + 0.02 ZnSO$_4$ + 0 .12 C$_4$H$_6$O$_6$ and 1.0 mol L$^{-1}$ Na$_2$SO$_4$ solutions and on Pt electrode (A) in the absence and (B) in the presence of tartaric acid.
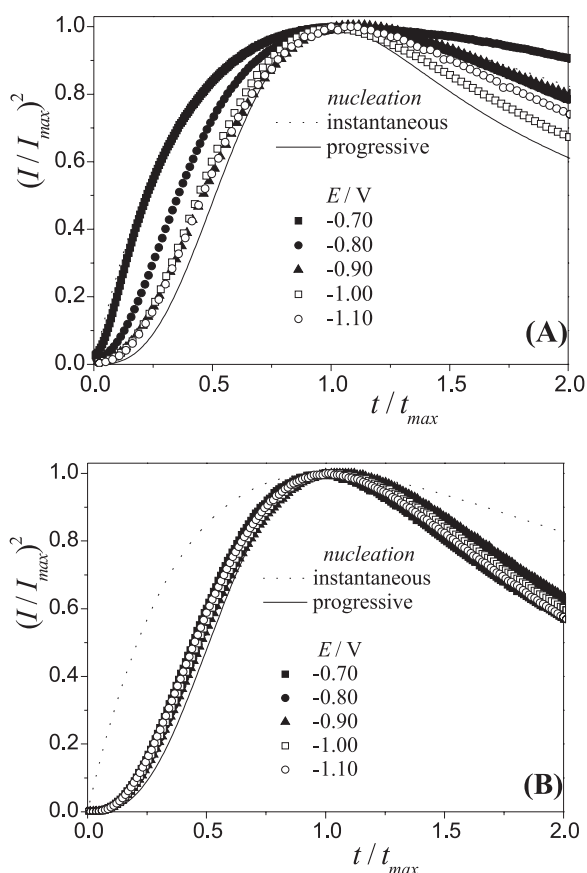
**Figure 5.** Non-dimensional plots, $(I/I_{max})^2$ vs. $t/t_{max}$, for instantaneous and progressive nucleation limiting cases. Points represent normalized experimental curves from current transients for Sn-Zn (A) in the absence and (B) in the presence of tartaric acid in the deposition bath.

**Figure 6.** Initial times of current transients with (A) $t^{1/2}$ and (B) $t^{3/2}$ in the absence of tartaric acid for Sn-Zn deposition.

Another diagnosis criterion given by the Scharifker and Hills nucleation model is based on the rising portion of the transient of current-time, in other words, on the analysis of the early stages of deposition. It is possible to represent (considering the initial transient portion) $I$ vs. $t^{1/2}$ for instantaneous, and $I$ vs. $t^{3/2}$ for progressive nucleation. Plots of $I$ vs. $t^{1/2}$ and $I$ vs. $t^{3/2}$ are presented in Figures 6 and 7 for Sn-Zn deposition in the absence and presence of tartaric acid, respectively.

In Figures 6 and 7 a better degree of linearity is obtained for $I$ vs. $t^{3/2}$ plot. Again, under the experimental conditions analyzed here, a progressive Sn-Zn alloy nucleation process occurs. In the absence of tartaric acid, the nucleation process may occur by instantaneous or progressive nucleation depending on the final potential. Plots of the rising portion of the transients show linear behavior with $t^{1/2}$ and $t^{3/2}$.

## Conclusions

Voltammetric results showed that tin deposition is favored by addition of tartaric acid due to the complex
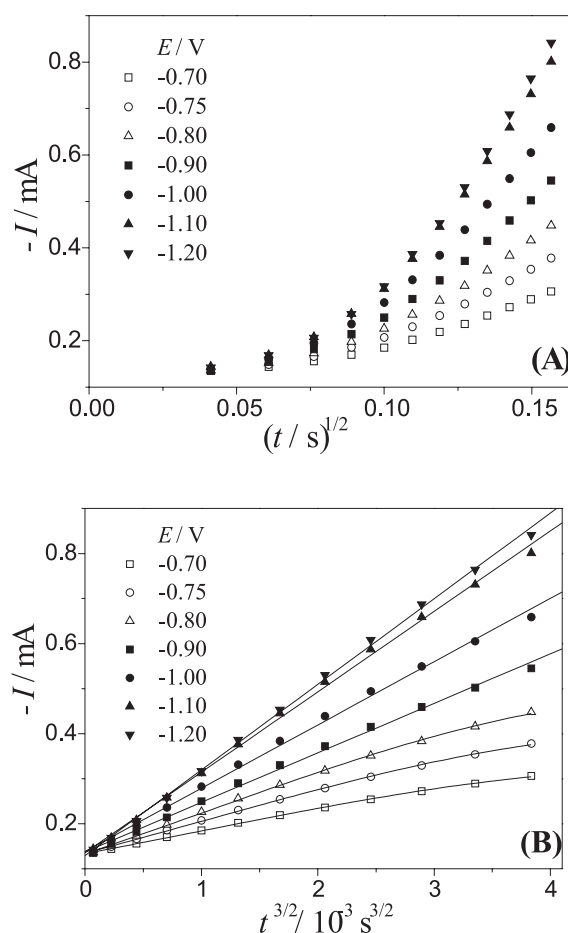
formed with this metal and tartrate anions. Comparing the dissolution charge in both baths, it can be concluded that tartrate also favors the reduction process in general.

SEM images shown that deposits morphology changes significantly with the deposition potential, but it is little affected by the presence of tartaric acid. In tartrade presence the deposits obtained are more uniform than in its absence. Zinc is incorporated to the deposit from -1.00 V to more negative potentials, changing significantly the morphology of the deposits. From EDX analysis it was possible to determine the atomic compositions of the alloys electrodeposited and it was concluded that the tartrate favors the zinc deposition at the most negative potential studied.

The experimental current transients were analyzed according to Scharifker and Hills models and with the results reported here it could be concluded that the electrodeposition of Sn-Zn alloy occurs *via* 3D multiple nucleation with diffusion-controlled growth. According to theoretical models, Sn-Zn alloy deposition in the presence of tartaric acid is governed by progressive nucleation. By the other hand, in the absence of tartrate the process
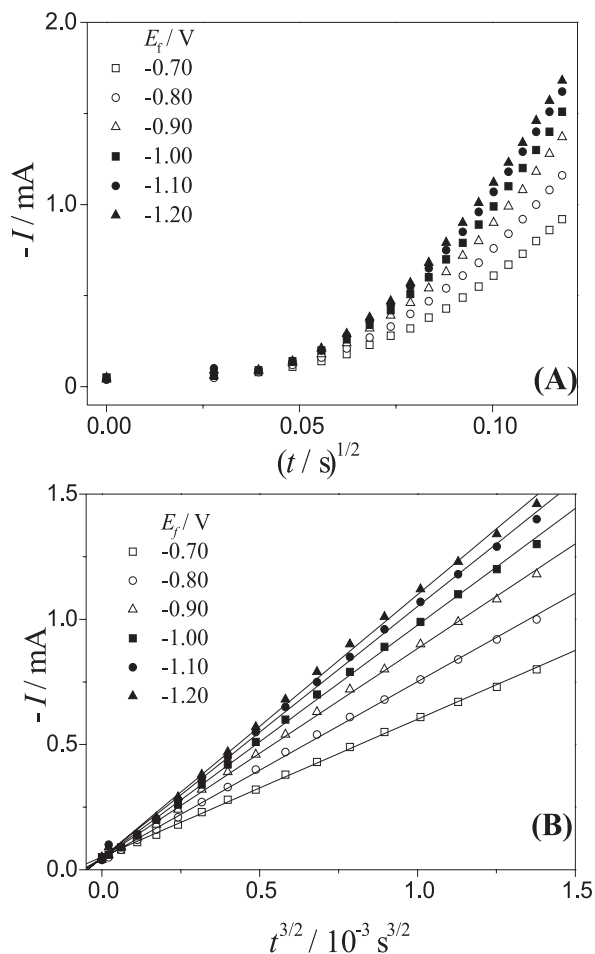
**Figure 7.** Initial times of current transients with (A) $t^{1/2}$ and (B) $t^{3/2}$ in the presence of tartaric acid for Sn-Zn deposition.

seems to change from instantaneous to progressive at more negative potentials, as soon as zinc is incorporated to the deposit.

## Acknowledgments

## References

1. Budman, E.; McCoy, M.; *Met. Finish.* **1995**, *93*, 10.

2. Vitkova, St.; Ivanova, V.; Raichevsky, G.; *Surf. Coat. Tech.* **1996**, *82*, 226.

3. Ashiru, O.A.; Shirokoff, J.; *Appl. Surf. Sci.*, **1996**, *103*, 159

4. Kohl, P.A.; *J. Electrochem. Soc.* **1982**, *129*, 1196.

5. Arai, S.; Akatsuka, H.; Kaneko N.; *J. Electrochem. Soc.* **2003**, *150*, C730.

6. Khaselev, O.; Zavarine, I.S.; Vysotskaya, A.; Fan, C.; Zhang, Y.; Abys, J.; *Trans. Inst. Met. Finish.* **2002**, *80*, 200.

7. Bentley, A.K.; Trethewey, J.S.; Ellis, A.B.; Cronew W.C.; *Nano Lett.* **2004**, *4*, 487.

8. Arai, S.; Watanabe, T.; *Mater. Trans. Jpn. Inst. Met.* **1998**, *39*, 439.

9. Beattie, S.D.; Dahn, J.R.; *J. Electrochem. Soc.* **2003**, *150*, C457.

10. Kang, S.K.; Buchwalter, S.; Tsang, C.; *J. Electron. Mater.* **2000**, *29*, 1278.

11. Guaus, E.; Torrent-Burgués, J.; *J. Electroanal. Chem.* **2005**, *575*, 301.

12. Guaus, E.; Torrent-Burgués, J.; *J. Electroanal. Chem.* **2003**, *549*, 25.

13. Vasantha, V.S.; Pushpavanam, M.; Muralidharan, V.S.; *Met. Finish.* **1996**, *94*, 60.

14. Abbott, A.P.; Capper, G.; McKenzie, K.J.; Ryder, K.S.; *J. Electroanal. Chem.* **2007**, *599*, 288.

15. Lin, K.L.; Sun, L.M.; *J. Mater. Res.* **2003**, *18*, 2203.

16. Wang, K.; Pickering, H.W.; Weil, K.G.; *Electrochim. Acta* **2001**, *46*, 3835.

17. Hu, C.C.; Wang, C.K.; Lee, G.L.; *Electrochim. Acta* **2006**, *51*, 3692.

18. Dubent, S.; De Petris-Wery, M.; Saurat, M.; Ayedi, H.F.; *Mater. Chem. Phys.* **2007**, *104*, 146.

19. Castrillejo, Y.; Garcia, M.A.; Martinez, A.M.; Abejon, C.; Pasquer, P.; Picard, G.; *J. Electroanal. Chem.* **1997**, *434*, 43.

20. Huang, J.F.; Sun, I.W.; *J. Electrochem. Soc.* **2003**, *150*, E299.

21. Scharifker, B.R.; Hills, G.; *Electrochim. Acta* **1983**, *28*, 879.

22. Correia, A.N.; Machado, S.A.S.; *J. Braz. Chem. Soc.* **1997**, *8*, 71.

23. Grujicic, D.; Pesic, B.; *Electrochim. Acta* **2002**, *47*, 2901.

24. Bento, F.R.; Mascaro, L.H.; *J. Braz.Chem. Soc.* **2002**, *13*, 502.

25. Yang, Z.N.; Zhang, Z.; Zhang, J.Q.; *Surf. Coat. Tech.* **2006,** *200,* 4810.

26. Bento, F.R.; Mascaro, L.H.; *Surf. Coat. Tech.* **2006**, *201*, 1752.

27. Bulhões, L.O.S.; Mascaro, L.H.; *J. Solid State Electrochem.* **2004**, *8*, 238.

28. Carlos, I.A.; Souza, C.A.C.; Pallone, E.M.J.A.; Francisco, R.H.P.; Cardoso, V.; Lima-Neto, B.S.; *J. Appl. Electrochem.* **2000**, *30*, 987.